Materials Today Physics 15 (2020) 100263

Contents lists available at ScienceDirect

Materials Today Physics

journal homepage: https://www.journals.elsevier.com/materials-today-physics

Ultra-high critical electric field of 13.2 MV/cm for Zn-doped *p*-type β-Ga_2O_3

E. Chikoidze [a, *], T. Tchelidze [b], C. Sartel [a], Z. Chi [a], R. Kabouche [c], I. Madaci [a], C. Rubio [d], H. Mohamed [a, e], V. Sallet [a], F. Medjdoub [c], A. Perez-Tomas [d, **], Y. Dumont [a]

[a] Groupe D'Etude de La Matière Condensée (GEMaC), Université Paris-Saclay, UVSQ, CNRS, 45 Av. des Etats-Unis, 78035, Versailles Cedex, France
[b] Department of Physics, Ivane Javakhishvili Tbilisi State University, 3 Av. Tchavtchavadze, 0179, Tbilisi, Georgia
[c] IEMN, CNRS, UMR8520, Av. Poincaré, 59650, Villeneuve D'Ascq, France
[d] Catalan Institute of Nanoscience and Nanotechnology (ICN2), CSIC and BIST, Campus UAB, Bellaterra, 08193, Barcelona, Spain
[e] Solid State Physics Department, National Research Center, El-Behooth St. 12311, Dokki, Giza, Egypt

ARTICLE INFO

Article history:
Received 15 July 2020
Received in revised form
4 August 2020
Accepted 11 August 2020
Available online 1 September 2020

Keywords:
Ultra-wide band gap
MOCVD growth
p type β-Ga_2O_3
Electrical properties
Critical electrical field

ABSTRACT

Which the actual critical electrical field of the ultra-wide bandgap semiconductor β-Ga_2O_3 is? Even that it is usual to find in the literature a given value for the critical field of wide and ultra-wide semiconductors such as SiC (3 MV/cm), GaN (3.3 MV/cm), β-Ga_2O_3 (~8 MV/cm) and diamond (10 MV/cm), this value actually depends on intrinsic and extrinsic factors such as the bandgap energy, material residual impurities or introduced dopants. Indeed, it is well known from 1950's that reducing the residual doping (N_B) of the semiconductor layer increases the breakdown voltage capability of a semiconductor media (e.g. as $N_B^{-3/4}$ by using the Fulop's approximation for an abrupt junction). A key limitation is, therefore, the residual donor/acceptor concentration generally found in these materials. Here, we report that doping with amphoteric Zinc a *p*-type β-Ga_2O_3 thin films shortens free carrier mean free path (0.37 nm), resulting in the ultra-high critical electrical field of 13.2 MV/cm. Therefore, the critical breakdown field can be, at least, four times larger for the emerging Ga_2O_3 power semiconductor as compared to SiC and GaN. We further explain these wide-reaching experimental facts by using theoretical approaches based on the impact ionization microscopic theory and thermodynamic calculations.

1. Introduction

Energy and power electronics rely on the capability of semiconductor solid-state devices to sustain high electric fields [1]. Such capability itself is determined by the semiconductor's fundamental property, band gap (Ɛg) and by the mechanism of the process leading to the breakdown. The breakdown phenomena -i.e. when highly resistive material under high electrical field start to conduct a current - is related with the process of impact ionization. It is customary to use the well-known unipolar Baliga's Figure of Merit, $\mu\varepsilon_r E_c^3$ to classify wide and ultra-wide bandgap semiconductors for power electronics [2,3]. A good semiconductor for power electronics should exhibit therefore large *critical electric field* (E_c) while keeping reasonably high free carrier mobility (μ) and dielectric constant (ε_r). In a parallel plate capacitor, containing an insulator media with no charges at the interfaces, the electric field is constant and the critical electric field is simply the breakdown voltage divided by the interplanar distance (i.e., $E_c = V_B/d$). In any semiconductor containing a certain doping (space charge), the electric field distribution is not constant anymore but it has a spatial distribution and maximum value which depend on the doping concentration itself. Already in 1966, Sze and Gibbons [4] proposed that for an abrupt (infinite) junction, the avalanche breakdown voltage (V_B) of any semiconductor is related to the drift region doping level (N_B) by the expression,

$$V_B = 60\left(\frac{\varepsilon_g}{1.1}\right)^{1/2}\left(\frac{10^{16}}{N_B}\right)^{3/4} \quad (0)$$

This qualitative expression already informs us that the breakdown capability depends on the free available charges (related to

* Corresponding author.
** Corresponding author.
E-mail addresses: ekaterine.chikoidze@uvsq.fr (E. Chikoidze), amador.perez@icn2.cat (A. Perez-Tomas).

https://doi.org/10.1016/j.mtphys.2020.100263
2542-5293/

native defects or dopants) but also on semiconductor's fundamental properties (such as bandgap energy ε_g) and the impact ionization parameters resulting in avalanche breakdown. Therefore, the effective critical electric field (defined as the breakdown voltage divided by the semiconductor depletion length), is actually depending on several geometrical and material quality factors. Regardless this fact, it is very usual to find in the literature values for the electrical critical field of the most popular power and wide bandgap dielectrics such as silicon (0.3 MV/cm), 4H−SiC (2.2 MV/cm), 2H-GaN (3.3 MV/cm), for β-Ga_2O_3 (8 MV/cm), diamond (~10 MV/cm) and AlN (12.7 MV/cm). To the best of the authors knowledge, in the case of β-Ga_2O_3, the *popular* value of 8 MV/cm (a value frequently given in the literature) was originally simply from an interpolation (it was indeed not calculated or measured experimentally) on the basis of a band gap energy model reported in 2012 [5]. Short after, further efforts in the theoretical front, corroborated a theoretically calculated critical electric field of 8 MV/cm (for undoped β-Ga_2O_3) [6]. Irudayadass and Shi [4], predicted a much larger electric field in the range of 9−17 MV/cm but it is largely anisotropic; i.e. depending on β-Ga_2O_3 crystallographic orientation [7]. They studied the plane directions [001], [100], [001], [−201] and observed that the theoretical maximum electric field was obtained for the [−201] crystallographic orientation. Experimentally, a record breakdown field of 5.2 MV/cm for β-Ga_2O_3/graphene heterostructures has been reported in 2018 while a year later it was reported up to 7 MV/cm for β-G_2O_3 grown on Si [8].

In this work, it is engineered, both, the out-of-plane crystallographic orientation and doping in order to maximize the blocking voltage capabilities of parallel-plane Ga_2O_3 capacitors grown on conductive Silicon substrates. To reduce the background impurity level of the thin-film, it is introduced Zn atoms (~0.5%) which results to be an amphoteric impurity. In short, *p*-type β-Ga_2O_3 doped by Zn critically decreases the impact ionization rate which results in the ultra-high experimental effective critical field of 13.2 MV/cm. One implication of our results is a further shift of the Baliga's figure-of-merit for the emerging ultra-wide bandgap β-Ga_2O_3 as compared to classical wide bandgap SiC and GaN, therefore reinforcing the enormous potential of gallium oxide for power electronics.

2. Kinetic impact ionization theory (KIIT)

The enhanced ultra-high critical electric field of p-type β-Ga_2O_3 is believed to be due to the combined effect of the ultra-low donor concentration and the further reduction of the impact ionization rate. In the following, it is used the Kinetic Impact Ionization Theory (KIIT) framework to understand the implications of acceptor dopant species. Under a sufficiently high electric field, the impact ionization phenomenon in a (low doped) semiconductor takes place when a high energy electron in the conduction band loses some of its energy by collision. This multiplication process results in three free carriers, two electrons and a hole, in place of the initial electron. Impact ionization by a hole is a similar process by which an energetic hole yields three final current carriers, two holes and an electron [9]. If the electric field is further improved, a multiplicative avalanche process may occur. At Impact ionization process is defined by impact ionization coefficients (α) which is the average number of ionizing collisions experienced by a carrier per unit distance of its travel in the direction of the electric field. . The semi-empirical Chynoweth [10] equation is often used as, $\alpha = ae^{-b/E}$ where E is the electric field and $a = \alpha_\infty$ [cm^{-1}] and b [V/cm] are material constants. A useful approximation is the one given by Fulop [11] or $a = cE^7$ (c being a constant). If one assumes the impact ionization of electron and holes to be the same, the avalanche breakdown for an abrupt junction using the Fulop's approximation results in the $N_B^{-3/4}$ dependence of eq. (0). Therefore, the avalanche breakdown occurs when the carrier concentration significantly increases in comparison the semiconductor's thermal concentration. Let's consider the impact ionization in wide band gap semiconductors. Due to wide band gap deep native donor/acceptor centers (if any), are assumed to deliver carriers during impact ionization. In terms of the microscopic parameters, in stationary state, the number of carriers is constant and determined by the following expression [12].

$$n\{\overline{\omega_i(E,T)} - \overline{\omega_r(n,E,T)}\} + n_0(E,T) = 0 \tag{1}$$

where $\overline{\omega_i}$and $\overline{\omega_r}$are the probabilities of impact ionization and recombination, averaged over distribution function, n_0 is the number of thermally ionized carriers. With increasing field $\overline{\omega_r}$ decreases, while $\overline{\omega_i}$ increases rapidly, resulting in a net carrier concentration enhancement. When $\overline{\omega_r} = \overline{\omega_i}$ carrier concentration goes to infinity and breakdown takes place. In the KIIT framework, the probability of impact ionization is proportional to the probability that the electron (hole) will cover without collision a path $l = \varepsilon_i/eE$, where ε_i is the activation energy of carriers from bound state of uncompensated donor or acceptor center [13]:

$$\overline{\omega_i} \sim \exp(-\varepsilon_i / elE) \tag{2}$$

The pre-exponential coefficient consists of concentration of neutral (filled) donor or acceptor centers from which carriers are activated - N_f, the capture cross section of this center σ_f, and velocity of the carrier u

$$\overline{\omega_i} = N_f \sigma_f u \exp(-\varepsilon_i / elE) \tag{3}$$

One may note that the probability of impact ionization $\overline{\omega_i}$ has the same electric field dependence as the Chynoweth equation with $b = \varepsilon_i/el$. The recombination coefficients also depend on concentration of ionized centersN_i, the capture cross section of this center σ_i, and velocity of the carrier u:

$$\overline{\omega_r} = N_i \sigma_i u \tag{4}$$

The capture cross section of ionized center$\sigma_i = \pi a_B^2$, where a_B is the Bohr radius of the center, which can be estimated by means of ionization energy; the capture cross section for the neutral center $\sigma_f = 20a_B/k$, where k is carrier wave vector [14],

Therefore, the critical field at which the breakdown occurs can be estimated by means of equating $\overline{\omega_r}$and $\overline{\omega_i}$:

$$E_{cr} = -\frac{\varepsilon_i}{el \ln\left(\frac{\pi a_B k}{20}\frac{N_i}{N_f}\right)} \tag{5}$$

which again is functionally identical to the Chynoweth law, $\ln\left(\frac{\alpha}{a}\right) = -\frac{b}{E}$. As seen from eq. (5), the critical field at which breakdown takes place depends on the ionization energy, (ε_i) and mean free path (l), and the density of neutral (filled) donor or acceptor centers from which carriers are activated [15].

3. Intrinsic and Zn-doped *p*-type Ga_2O_3, a review

Here, we propose a strategy for the enhancement of the *p*-Ga_2O_3 critical electric field by shortening the mean free pass of free carriers (l). For achieving that in practice, we further introduce dopant atoms in Ga_2O_3. The selection of the dopant species is very

particular: (i) *a dead acceptor* it should not lead to an increase of free carriers (as otherwise is the usual situation when doping a semiconductor) and (ii) *while as a donor* it should not lead to a change of conductivity type (i.e., keeping the *p*-type native conductivity of our Ga_2O_3).

We chose the amphoteric deep impurity II group element Zinc (Zn) to this end. Zn doping related theoretical predications are rather controversial. Zn doping (~2%) does not change the basic electronic structure of β-Ga_2O_3, but only generates an empty energy level above the maximum of the valence band, which is shallow enough to make the Zn-doped β-Ga_2O_3 a typical *p*-type semiconductor [16]. However, for C. Zhang and coauthors, an atomic Zn concentration of ~4% has been estimated to introduce shallow levels above the valence band at around 0.3 eV [17]. Contrary to this statement, for ~1.5% doping, Zn has been reported to be a very deep acceptor with >1.2 eV energy level above valence band maximum [18] with low activation rate [19]. Co-doping Zn—N has been reported as well, and refereeing an acceptor with possibly 0.5 eV activation energy [20]. Even ferromagnetic order has been predicted by 3.5 wt% Zn doping leading 100% spin polarization in gallium Oxide [21].

There are some experimental works dedicated to high amount (>1%) Zn incorporation into Gallium Oxide for different purposes (as summarized in Table 1). W. Yue et al. studied the effect of Zn doping (2 wt%) by magnetron sputtering showing that with Zn doping the band gap slightly was reduced from 4.90 to 4.87 eV [22]. Similarly, it was found that with the increase of Zn dopant concentration up to ~3%, the crystal lattice expands, the energy band gap shrinks, and the oxygen vacancy concentration decreases [23]. Tao et al. [24] reported however that the rise in Zn doping contents is accompanied by a widening the band gap due to Burstein-Moss effect. Interestingly, in Zn-(β-Ga_2O_3) thin films, electrical characterization by Hall effect at room temperatures show an electron concentration decreases from 2×10^{14} to 6×10^{12}cm^{-3} with increasing the nominal Zn content from 0 to 7 at%, showing that Zn plays acceptor role. From cathodoluminescence measurements the acceptor level of Zn_{Ga} is estimated to be 0.26 eV above the valence band maximum [25]. Zn doping of gallium oxide was done for improvement of oxygen gas sensing properties: it was observed that *n*-Ga_2O_3 doped with Zn showed increase of resistivity at $T < 450$ °C [26].

Agnitron Technology Incorporated (USA) reported β-Ga_2O_3 Zn doped thin films on c-sapphire by MOCVD the incorporation of 10.9% Zn XRD patterns yielded to a mono-phase polycrystalline structure with increase of lattice parameters with doping, though room temperature Hall measurements were not successful due to very high resistivity of the samples [30]. Recently, we have shown that incorporation of Zn in *p*-type β-Ga_2O_3 with more than 5% leads the transformation of orthorhombic structure into spinel $ZnGa_2O_4$ with an increased band gap (~0.2 eV) and *p*-type carrier densities ($\times$ 10-100 cm^{-3}) [29].

Very few experimental works are reported about low doping cases, when incorporated Zn amount is less than 1%. Shrestha et al. [31] studied properties of 0.59% Zn doped Ga_2O_3 nano-porous layers for photo-induced hydrogen generation. It has been concluded that a presence of small amount of zinc doping in Ga_2O_3 can reduce trapping sites at the donor level under the conduction band, and thereby increase the mobility of electrons. On the other hand, zinc doping also creates additional trapping sites as acceptor level over the valence band, which hampers the activation of holes. An improvement of photocatalytic activity by Zn doping (up to 1 atomic % of zinc) on H_2O splitting is found and associated with increase in the mobility and concentration of holes due to the formation of an acceptor level [32]. Another study on monocrystalline Zn doped β-Ga_2O_3 nanowires/*n*-type β-Ga_2O_3 junction, shows good rectifying behavior, suggesting that the Zn doped β-Ga_2O_3 nanowires are of *p*-type conductivity [33]. A summary of previously reported in the literature the native and Zn- acceptor centers *in* Ga_2O_3 is shown in Table 1.

Zn as an II group element is expected to be an acceptor in Ga_2O_3, though due to its smaller atomic radius, (137 pm) in comparison to Ga (153 pm), it can occupy an interstitial position as well and acts as a donor. This amphoteric nature of Zn could be an origin of possible so-called "impurity auto-compensation" effect. The problem of auto-compensation was discussed by Kroger [34] for Li doped ZnO, while Zn amphoteric nature has already been reported in GaAs [35].

4. Thermodynamic analyses of Zn:Ga_2O_3

From the thermodynamically point of view, using Kroger-Vink notations, the following equilibrium relationships with the corresponding mass action laws are considered:

(i) Lattice thermal ionization

$$\varnothing \leftrightarrow e + h, \qquad K_g = np \tag{6}$$

(ii) Substitutional Zn transfer to interstitial position

$$Zn_{Ga} \leftrightarrow Zn_i + V_{Ga}, \quad K_{Zn} = \frac{[Zn_i][V_{Ga}]}{[Zn_{Ga}]} \tag{7}$$

(iii) Donor and acceptor impurity ionizations

Table 1
A summary of previously reported intrinsic and Zn-doped *p*-type Ga_2O_3 from the literature; [a]measured at 300K; [b]measured at 850K; [c]low p-type resistivity attributed to charge carrier multiplication via collective excitation of aggregated excitons and/or electron-hole liquid; [d]amorphous silicon; [e]Overall reduction of conductivity/Zn considered as an acceptor; [f]determined by cathodoluminescence for nanowire; Zn-content stabilized in a spinel $ZnGa_2O_3$ structure.

Year	Autor	Zn [%]	Substrate	Growth	Type	p [cm^{-3}]	μ_h [cm^2/Vs]
2017	Chikoidze [27]	0	(0001) sapphire	PLD	p-type	2×10^{13}[a]	0.2
2019	Chikoidze [28]	0	(0001) sapphire	MOCVD	p-type	6×10^{14}[b]	9.6
2003	Li Y [26]	9.7—24.7	a-Si[d]	PE-ALD	n-type	Zn acceptor[e]	–
2012	Yue [22]	2.0	Si (111)	RF sputtering	–	–	–
2013	Shrestha [32]	0.59	Ga, GaZn alloy	anodization	–	–	–
2014	Wang [25]	0.0—7.0	(0001) sapphire	PLD	–	$E_a = 0.26$eV[f]	–
2016	Feng [34]	1.3—3.6	NW[g]/β-Ga_2O_3	CVD	–	Zn acceptor	–
2017	Alema [30]	10.9	(0001) sapphire	MOCVD	–	–	–
2017	Guo [23]	0.69—3.03	(0001) sapphire	Magnetron sputtering	n-type	Zn acceptor	–
2020	Chikoidze [29]	32[i]	(0001) sapphire	MOCVD	p-type	2×10^{15}[b]	10
2020	This work	0.5	(0001) sapphire	MOCVD	p-type	1×10^{14}[b]	2

$$Zn_{Ga} \leftrightarrow Zn'_{Ga} + h, \quad K_a = \frac{\left[Zn'_{Ga}\right]p}{[Zn_{Ga}]} \tag{8}$$

$$Zn_i \leftrightarrow Zn_i^{\bullet} + e, \qquad K_d = \frac{[Zn_i^{\bullet}]n}{[Zn_i]} \tag{9}$$

(iv) Ionization of native acceptor, gallium vacancy

$$V_{Ga} \leftrightarrow V'_{Ga} + h, \quad K_A = \frac{\left[V'_{Ga}\right]p}{[V_{Ga}]} \tag{10}$$

(v) Interaction with environment, gas phase:

$$\frac{3}{2}O_2(gas) \leftrightarrow O_O + 2V_{Ga} \quad , K_{V_{Ga}} = \frac{[V_{Ga}]^2}{P_{O_2}^{3/2}} \tag{11}$$

here e and h denote electron and hole, n and p their concentrations. Zn_{Ga} and Zn_i denote Zn atoms in substitutional and interstitials sites, respectively, while $[Zn_{Ga}]$ and $[Zn_i]$ are their concentrations. $Zn'_{Ga}$and $Zn_i^{\bullet}$ denote ionized acceptor and donor impurities, while $[Zn'_{Ga}]$ and $[Zn_i^{\bullet}]$ are their concentrations. V_{Ga} denotes a Gallium vacancy, $[V_{Ga}]$ is the Gallium vacancy concentration, V'_{Ga} is one ionized galium vacancy and $[V'_{Ga}]$ its concentration. Equations 6–11 together with electro-neutrality condition

$$\left[Zn'_{Ga}\right] + \left[V'_{Ga}\right] + e = [Zn_i^{\bullet}] + p \tag{12}$$

and mass balance equation

$$\left[Zn'_{Ga}\right] + [Zn_i^{\bullet}] + [Zn_{Ga}] + [Zn_i] = [Z_{tot}] \tag{13}$$

establish the equilibrium concentrations of electrons and holes, as well as impurities and defects in different charge states. Electro-neutrality and mass balance depend on the total Zn concentration ($[Z_{tot}]$), temperature (T) and pressure (P_{O_2}) in surrounding atmosphere.

We calculated the concentration of these spices for fixed temperature (T = 750 °C) and total pressure (30 tor) in the chamber reactor (these are the parameters we use in experiment) versus Zn total concentration. As usual, few additional assumptions on the three hypothetical ranges of impurity concentration are considered [36]: (I) The range of *intrinsic conductivity* – in this range the total concentration of Zn is very low- and dominant species is one-charged intrinsic acceptor V'_{Ga} and hole. (II) The range of *impurity p-conductivity* – with the increase of Zn concentration gallium vacancies might be occupied with Zn atoms; so dominant terms in eq. (12) are $[Zn'_{Ga}]$ and$p$. (III) In the range of *impurity auto-compensation* – with further increase of Zn concentration - a fraction of Zn atoms occupies interstitial sites. In this range dominant species are $[Zn'_{Ga}]$ and $[Zn_i^{\bullet}]$. Such approximations provide a clear picture of doping peculiarities and simplify the calculations. The boundaries between these ranges can be defined by means of discontinuity of concentrations charge carriers or other species.

In the first region (*I: intrinsic region*),

$$p = \left[V'_{Ga}\right] = \left(K_A K_{V_{Ga}}^{1/2} P_{O_2}^{3/4}\right)^{1/2} \tag{14}$$

In the second region (*II: impurity p-type*),

$$p = \left[Zn'_{Ga}\right] = [Zn_{tot}] \tag{15}$$

In the third region (*III: impurity auto-compensation*)

$$p = \left(\frac{K_a K_g K_{V_{Ga}}^{1/2} P_{O_2}^{3/4}}{K_d K_{Zn}}\right)^{1/2} \tag{16}$$

The boundary between the first and second region corresponds to

$$[Zn_{tot}]_{I-II} = \left(K_A K_{V_{Ga}}^{1/2} P_{O_2}^{3/4}\right)^{1/2} \tag{17}$$

And the boundary between the second and the third region

$$[Zn_{tot}]_{II-III} = \left(\frac{K_a K_g K_{V_{Ga}}^{1/2} P_{O_2}^{3/4}}{K_d K_{Zn}}\right)^{1/2} \tag{18}$$

This boundary concentration indicates the efficiency of doping. If this concentration is very small, that is if impurity auto-compensation starts at low concentration, it is obvious that doping cannot increase p-conductivity.

In our case $[Zn_{tot}]_{I-II}$ and $[Zn_{tot}]_{II-III}$ are approximately the same ($\approx 10^{14}$ cm^{-3}), therefore we do not have a sizable region where impurity controls the conductivity. In fact, the concentration of holes in Zn-doped samples is even less than that in undoped samples. In general, the total hole concentrations $[Zn_{tot}]_{I-II}$ and $[Zn_{tot}]_{II-III}$ do depend on temperature. As shown in Fig. 1, the region in between $[Zn_{tot}]_{I-II}$ and $[Zn_{tot}]_{II-III}$ is further narrowing with increasing the temperature. Very relevantly, $[Zn_{tot}]_{II-III}$ remains low at the whole temperature range. This fact indicates that, in Zn-doped β-Ga_2O_3, auto-compensation (due to the amphoteric nature of Zn) is very strong. In practice, it is very challenging to select the optimal temperature and Zn concentration, which can provide the impurity controlled p-conductivity.

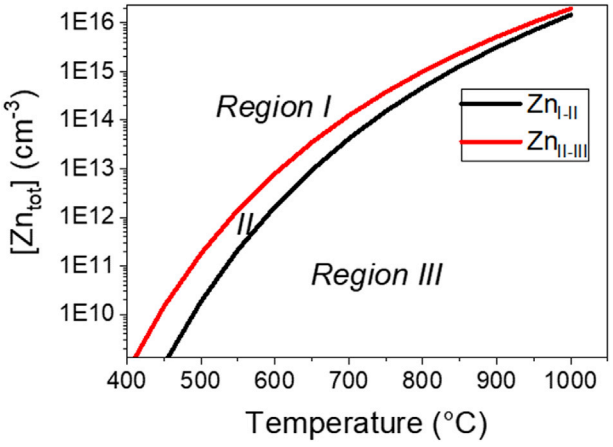

Fig. 1. Phase diagram of intrinsic *I*, impurity p-type *II*, and impurity auto-compensation *III* regions, with boundary curves (I-II in red, and II-III in back) versus temperature for P_{tot} = 30 torr.

5. *p*-type Ga_2O_3 on conductive silicon substrates

5.1. Structural properties

To evaluate the electrical breakdown voltage in vertical structure and effective critical electric field, Zn-doped β -Ga_2O_3 films were grown on conductive *n*-type Si (111) substrates. For comparison, Zn-doped β -Ga_2O_3 films were grown on insulating *c*-sapphire, to evaluate electrical transport properties (carrier, mobility). The layers were grown at low pressure (30 torr) in a horizontal MOCVD reactor. The Ga/O ratio and growth temperature were fixed to 1.4×10^{-4} and 775 °C respectively. Total pressure of oxygen were used as 5.5 Torr and 12 Torr. Zn flux was varying between 0 and 3.8 μmol. By adjusting the growth parameters, the layer thickness (systematically measured by SEM) was varying in the range of 200–400 nm for both substrate case, having similar growth rates.

On sapphire, the Zn doping does not change the quality of (−2 0 1) textured layers. X-ray (Cu-Kα) diffractograms, recorded between $2\theta = 10°$ and 130°, in $\theta/2\theta$ configuration, exhibit a highly (−2 0 1) texture of undoped and Zn:β-Ga_2O_3 phase with monoclinic space group (*C*2/m) symmetry (Fig. 2-a). The new and interesting for us was deposition on Si substrate. Several studies have shown that, as well as substrate of sapphire, silicon wafer can be used for Ga_2O_3 growth. MOCVD is one of effective methods using for deposition of Ga_2O_3, it's usually chosen for its reproducibility, film adherence [37], scalability into larger commercial systems, and applicability to current device technology [38–43], while another techniques such as PEALD [8], sputtering [44,45], also were used for Ga_2O_3 on silicon. Obtained film quality are varying from amorphous to polycrystalline, depending on growth technique, deposition temperature and post annealing procedure. Our undoped and doped films deposited on Si (111) are of comparable quality to state-of-the art Ga_2O_3 films grown on sapphire (0001) with [−2 0 1] preferential normal direction (Fig. 2-b). Additional tiny Bragg peaks, intensity ratio lower than 1/30) are detected with random orientations. SIMS measurements have shown that there is only samples grown by the maximum flux 3.8 μmol had detectable level of Zn atoms. Estimated concentrations for both substrates are very similar: $[Zn] = 1.5 \times 10^{19}$ at/cm^{-3} for Ga_2O_3 on sapphire (0001) and $[Zn] = 3.2 \times 10^{19}$ at/cm^{-3} for Ga_2O_3 on Si (111), which is about 0.5% of doping level. This value agrees very well with the value extracted from energy-dispersive X-ray spectroscopy (EDX) profile from a transmission electron microscopy (TEM) measurements performed on the Zn:Ga_2O_3/Si sample. According to EDX, there is a thin SiO_2 layer (2–3 nm) at the β-Ga_2O_3/Si interface, which is well seen by TEM picture. Fig. 2-c. By TEM we can saw an amorphous layer (15–20 nm) on top of SiO_2. EELS profiles show that there is no diffusion of Si in this upper amorphous layer, and it has the same chemical composition Zn:Ga_2O_3 with Zn = 0.5%.

5.2. *p*-type Ga_2O_3 electrical transport properties

While the breakdown measurements take advantage of the conductive silicon substrate, a detailed study of the β -Ga_2O_3's

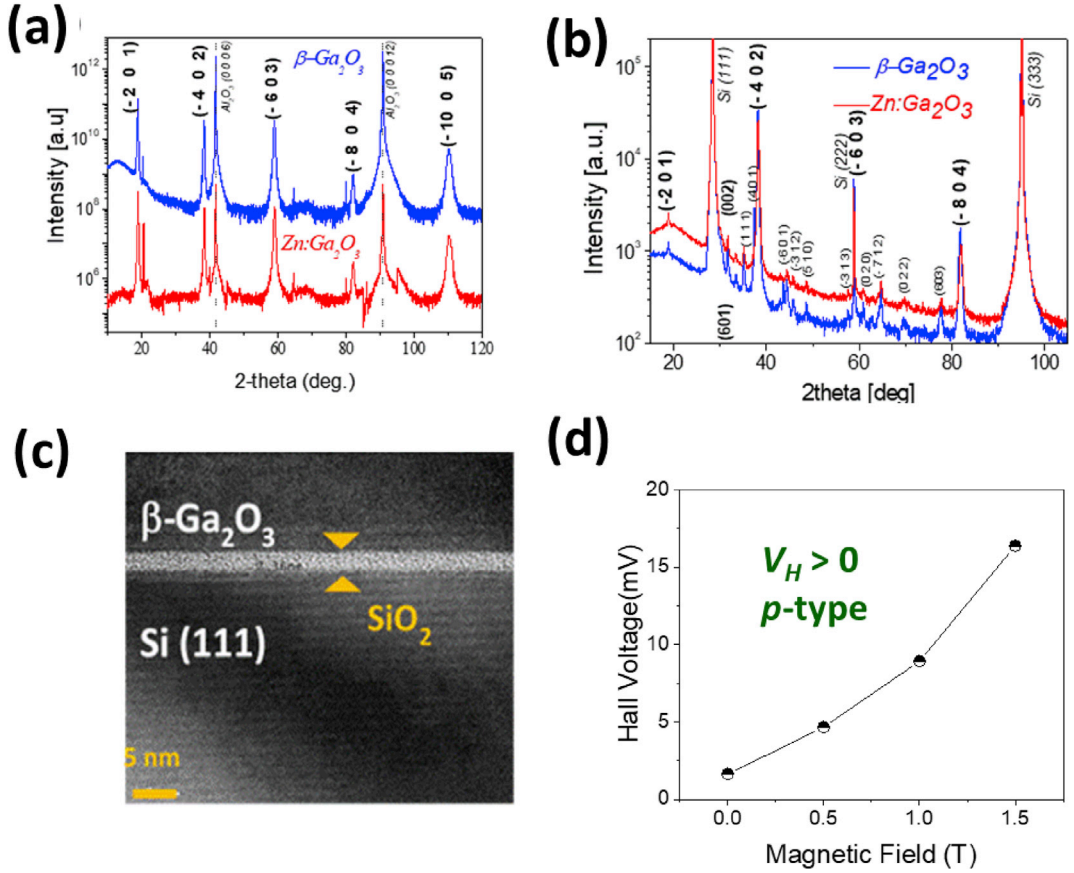

Fig. 2. Cu-Kα X-ray diffractograms β -Ga_2O_3 and β -Zn:Ga_2O_3films deposited by MOCVD on (a) Al_2O_3 (0001) and (b) Si (111) substrates; (c) Transmission electron microscopy of the film on Si (111). Amorphous natural SiO_2 2–3 nm thick layer is evidenced at interface. d) Hall voltage, V_H versus applied magnetic field for T = 850K. Positive sign of V_H confrims the p-type conductivity.

electrical transport properties have been performed on the samples grown on insulating substrate (Sapphire). I–V curves showed Ohmic behavior. Hall Effect measurements in Van der Pauw configuration is used to determine the resistivity, carrier type, density and mobility. Resistivity for undoped Ga_2O_3 (grown by 5.5 Torr total oxygen pressure) at T = 530 K (the lowest temperature for valid measurements) was found to be $\rho = 2.9 \times 10^5$ Ω cm; and by heating the sample up to T = 850 K resistivity decreases down to $\rho = 1.2 \times 10^3$Ω cm (Fig. 3-a). ρ(T) dependence shows normal behavior of semi-insulating material, with enhancement of contribution of hopping conductivity below T < 650K (Fig. 3-a). Zn doped sample exhibits much higher resistivity up to $\rho = 2 \times 10^7$ Ω cm for T = 550 K. From ln (σ) versus 1/T plot a conductivity activation energy were determined very close for both samples, around $\varepsilon_a = 1.24 \pm 0.05$ eV. To validate the sign of conductivity type in the material we usually follow the procedure described in Ref. [28]. In non-magnetic material, V_H is linearly proportional to applied magnetic field and positive sign indicates that the majority charge carriers are p-type (holes). We systematically have performed Hall voltage measurements at varying magnetic fields (0–1.5 T) for undoped and doped samples and in both of cases $V_H > 0$ positive Hall voltages were detected, indicating that majority carriers are holes. See Fig. 2(d) for $Zn:Ga_2O_3/Al_2O_3$ sample. The detailed Hall Effect measurements for undoped sample: carrier concentration, type and mobility (At 850 K, $p = 5.6 \times 10^{14}$ cm-3 mobility varies between 9.6 and 8.0 cm^2/V in 680–850 K temperature range) have been reported by us in Ref 28. Additionally, for present work we have studied electrical properties for undoped sample The growth conditions we have investigated are primarily oxygen total pressure and Zn-flux. Oxygen total pressures were adjusted to be 5.5 Torr (low) and 12 Torr (high). Zn flux was varying between 0 and 3.8 μmol. The best conditions in terms of breakdown were observed to be low pressure growth and 0.5%Zn content. Undoped sample grown at high oxygen total pressure of 12 Torr exhibited 10 times higher carrier concentration, $p = 6 \times 10^{15}$ cm^{-3} than the sample grown at 5.5 Torr pressure, which can be explained by thermodynamic equilibrium of native defects favorable for V_{Ga} creation, responsible for free hole creation.

Hall Effect measurements for $Zn:Ga_2O_3/Al_2O_3$ (0001) was more complicated to perform in whole temperature range. Fig. 3(C) shows Hall hole carrier concentration versus T for undoped and 0.5% Zn-doped β-Ga_2O_3 thin films. High temperature (700–850 K) Hall Effect shows slight decrease of hole concentrations, $p = 1 \times 10^{14}$ cm^{-3} at 850 K. indeed, if auto-compensation mechanism takes place, Zn dopant cannot increase of p -type conductivity, even more, as we see in experiment, "amphoteric" nature of Zn can lead a decrease of charge carriers. This result corresponds well to the thermodynamic calculations discussed above. As it is shown in Fig. 3, undoped and Zn-doped samples reveal *p*-type conductivity at high temperature exhibiting both the same activation energy of E_a ~1.2 eV. The free hole concertation at room temperature was estimated to be $< 1 \times 10^8 cm^{-3}$. Ga_2O_3 Hall holes mobilities for doped sample are lower, μ = 1–2 cm^2/V. Such decrease of hole mobility is not surprising and might be related with doping leading the increase of scattering on Zn impurities, consequently shortening of mean free pass of free carriers.

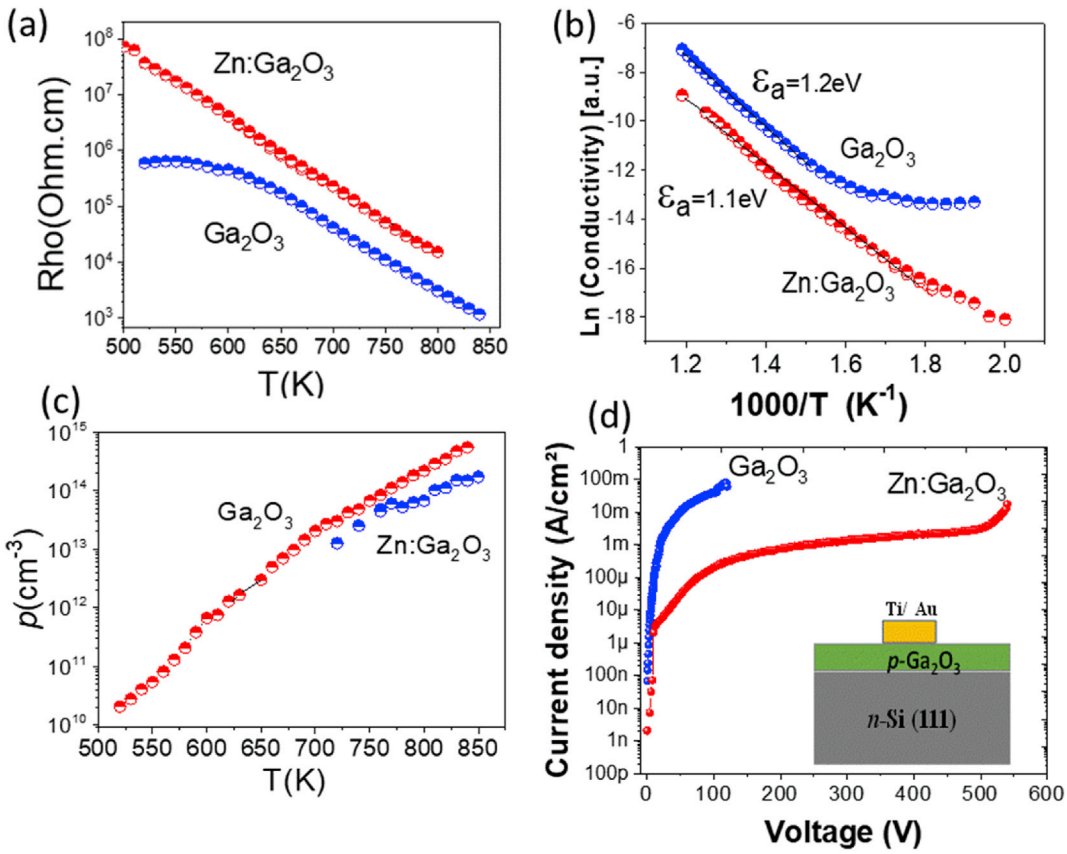

Fig. 3. (a) Resistivity versus temperature (b) ln(conductivity) versus 1000/T; (c) Hall hole carrier concentration versus T for undoped and 0.5% Zn-doped β-Ga_2O_3 thin films d) I–V curves for breakdown voltage measurements for undoped Ga_2O_3/Si (111) and 0.5% $Zn:Ga_2O_3$/Si (111) structures. Insert: sketch of the vertical p-n heterojunction structure with Ti(400 nm)/Au(200 nm) contacts.

5.3. p-type Ga_2O_3 critical electric field

Vertical parallel plane capacitors have been fabricated by depositing Ti(400 nm)/Au(200 nm) contacts onto the undoped and Zn doped p-Ga_2O_3 grown on the conductive Si substrates, (see inset of Fig. 3-d). The vertical breakdown voltage was determined to be 60V for 270 nm thick undoped p-Ga_2O_3/Si (grown by 12 Torr oxygen pressure) having $p = 6 \times 10^{15} cm^{-3}$ hole concentration contrary to 124 V for the undoped p-Ga_2O_3/Si for 200 nm thick (grown by 5.5 Torr oxygen pressure) with $p = 5 \times 10^{14} cm^{-3}$ hole concentration. Consequently, defined corresponding critical electrical fields are $E_C = 2.2$ MV/cm and $E_C = 5.7$ MV/cm. This is a confirmation that E_c strongly depends on free carrier concentration in the material, as is expected from formula (0) stated in the Introduction. For p-Zn:Ga_2O_3/n-Si structure (where Zn:Ga_2O_3 was grown at low, 5.5 Torr oxygen pressure we have measured 540 V breakdown voltage. A bare Si substrate with a native SiO_2 (2–3 nm thick layer) has been characterized as well. The vertical breakdown voltage (around 10V) is determined to produce negligible contribution to the large experimental V_{BR} of the *p*-Ga_2O_3/Si structure. Taking into account the experimentally (by SEM) determined TEM of 200 nm (Ga_2O_3) and 400 nm (Zn:Ga_2O_3), and extracting bare substrate related V_{BR} the effective parallel plate critical electric field was determined to be $E_C = 5.7$ MV/cm for Ga_2O_3 and $E_C = 13.2$ MV/cm, for Zn:Ga_2O_3 respectively. To be certain of this breakthrough value for gallium oxide, we suspected a contribution of the amorphous Zn:Ga_2O_3 layer (20 nm) on the top of SiO_2 layer, mentioned in section 5. Although we didn't observed Si (very efficient dopant in Ga_2O_3) at this interface by EDX profile, we estimated an undervalue associated to the contribution of a 20 nm thick layer with a 30 MV/cm critical field. So Ec = 13.2 (−0.9) MV/cm. The extraordinary experimental critical electrical field value of 13.2 MV (almost twice the largest breakdown electric field of ~7 MV/cm previously reported [7] for Ga_2O_3 to the best of our knowledge) is believed to be due to the Zn-doped *p*-type nature of the β-Ga_2O_3; the origin of the delayed impact ionization rate are the deep and amphoteric nature of Zn-dopants and the smaller hole mean free path (i.e., Zn-dopant makes the film even more insulating). In the following we, use the KIIT framework to test this assumption (eq. (5)). It should be mentioned that the experimental KIIT parameters (as carrier concentrations and mobilities) are from Hall Effect measurements performed on undoped Ga_2O_3 and Zn:Ga_2O_3 on Al_2O_3(0001) insulating substrates. Hall Effect measurements were not possible to carry out for the samples grown on much conducting Si substrates. As mentioned above, as determined from SIMS, the incorporation of Zn is very similar for Ga_2O_3 grown on Al_2O_3 and Si substrates. Besides, there is no critical structural and morphological differences of these films grown either on sapphire or silicon, consequently the transport properties are assumed to be comparable. Avalanche breakdown process and consequently critical electrical filed value as it is seen from formula (5) depends N_i / N_f ratio and mean free pass of carriers, l. The concentration of ionized centers N_i is assumed to be equal (when high electrical field is applied) to the free carrier concentrations, which, can be estimated from the experimental value of the current density when breakdown occurs: I = 10 μA for Ga_2O_3/Si and 100 μA for Zn:Ga_2O_3/Si. Consequently, N_i ~$10^{13} cm^{-3}$ and N_i~$10^{14} cm^{-3}$ for Ga_2O_3 and Zn:Ga_2O_3, respectively. N_f is a concentration of neutral (filled) defects which are a source of free carriers, thus in our case it is considered the number of gallium vacancies. It is assumed to be approximately equal to total concentration of vacancies, which approximately equals to the high temperature hole concentration 10^{14}-10^{15} cm^{-3}. Then, we estimate the mean free pass of carriers (holes) using experimentally measured values of Hall mobilities. The mean free path is given by $l = V_{thermal} \times \tau$, where $V_{thermal}$ is an average thermal velocity of free carriers at low electrical field and τ is the scattering rate of free carriers. Assuming that $V_{thermal} = \sqrt{3k_BT/m_h^*}$, the scattering rate τ can be determined from the Drude model $\mu = e\tau/m_h^*$. Therefore, the mean free path can be calculated as $l = e^{-1}\mu\sqrt{3k_BTm_h^*}$. At 850K, the experimental hole mobility was found to be 1 cm^2/Vs and 8 cm^2/Vs for the Zn-doped and the undoped samples, respectively. The hole effective mass value m_h^* for different crystallographic orientations has been given in the literature. According to density functional theory (DFT) calculations from Mock et al. [46], the hole effective mass is fairly anisotropic in $\vec{a}$, $\vec{b}$ *and* $\vec{c}$ directions: $m_{h,a}^* = 1.77\ m_0$; $m_{h,b}^* > 10\ m_0$; *and* $m_{h,c}^* = 0.41\ m_0$. For our estimations, we take a mean value of hole effective mass in $(\vec{a}, \vec{c})$ plane concerning both Hall measurements and vertical Breakdown: $m^* = 3 \times (1/m_a + 1/m^2_b + 1/m^3)^{-1} = 4.65\ m_0$. We then estimate a mean free path of l (β-Ga_2O_3) = 3.1 nm and l (Zn:Ga_2O_3) = 0.37 nm, for the undoped and Zn-doped Ga_2O_3 *p*-type semiconductors. Thus, the mean free path is eight times smaller for doped Zn: Ga_2O_3 when compared to the undoped case. Since breakdown was experimentally measured at room temperature, we estimated room temperature mean free path considering that in Ga_2O_3 mobility follows $\mu \sim T^{-3/2}$ law [47]. In should be mentioned, that motilities decrease in high electrical field, when carrier velocity tends to saturate, thus in reality mean free paths should be even shorter at room temperature. Once determined the mean free path, concentration of ionized centers N_i and the number of neutral gallium vacancies N_f, we can revisit the microscopic kinetic impact ionization theory. The critical electrical field values where given by $E_c = (E_a/el)\ln[\pi a_0 k N_i/20N_f]$. According to the KIIT model the calculated critical electric field lies in the range of 2 MV/cm and 5.7 MV/cm for the undoped Ga_2O_3 and Zn-doped Ga_2O_3, respectively. The discrepancy with the experimental values (5.7 MV/cm and 13.2 MV/cm for undoped and Zn-doped Ga_2O_3) may come from the inaccuracy of the hole effective mass value or/and the room temperature interpolation of hole mobilities. Although quantitively inaccurate, a microscopic model of kinetic impact ionization based in hole activated impact ionization qualitatively explains the root reason of the extraordinary capability of Zn-doped *p*-type Ga_2O_3 to sustain very large electric fields.

6. Conclusions

During many years, metal oxides in solid-state electronics were primarily well known for their outstanding insulating properties. Recently, due to a greater control of the conductivity and the possibility of achieving high-quality large crystals (up to 6-inch), wide and ultra-wide oxide semiconductors have attracted a lot of interest in applications such as power electronics. In this work, capability of p-type undoped Ga_2O_3/Si material to sustain high E_C = 6.0 MV/cm critical electrical field is shown experimentally for the first time. We have demonstrated also an efficient strategy for enhancement of E_C by Zn-doping up to 13.2 MV/cm, which is 65% larger than the frequent theoretical maximum value found in the literature (8 MV/cm). According with the kinetic impact ionization theory and thermodynamic calculations, doping with 0.5% amphoteric Zn a *p*-type Ga_2O_3 thin-film further reduces the free holes concertation and their mean free path, thus delaying the impact ionization phenomena. Notably, the experimental critical electric field for polycrystalline Zn:Ga_2O_3 thin films found in this work is to be ~4 times the one from SiC and GaN. Also it already surpasses widely adopted theoretical value (~10 MV/cm) for

Diamond. This result gives a clear proof of the enormous potential of gallium oxide for power electronics, and hopefully it will also stimulate researchers for calculations and measurements of impact ionization coefficients for this fascinating material.

7. Experimental and theoretical methods

In order to study the role of incorporated Zn (<1%) and its effect on point defects and free carrier concentrations, the thermodynamic equilibrium in the Zn:Ga $_2O_3$ (crystal) -versus- O_2 (gas) system was modeled. We have defined the dependence of point defects and charge carriers on both temperature and oxygen partial pressure in the surrounding atmosphere. The analysis was made using the Kroger method of quasi-chemical equations, described in details for undoped Ga_2O_3 in our previous report [27].

Undoped and Zn doped Ga_2O_3 films on sapphire (0001) and n-type Si (111) substrates. The layers were grown at low pressure (30 torr) in a horizontal MOCVD reactor with separate inlets to avoid premature reactions in the manifold between di-oxygen and organometallics precursors. Tri-methyl-gallium (TMGa) and di-oxygen were used as precursors for gallium and oxygen respectively. Argon was used as carrier gas. The TMGa bubbler was fixed at −15 °C in order to obtain to low growth rate around 5 nm/min. Layer's thicknesses were varying between 200 nm and 400 nm. The growth of Ga_2O_3 on both substrates exhibited similar growth rates. By adjusting the growth parameters, the layer thickness (systematically measured by SEM) was adjusted between values in range 200–400 nm for both substrates (Si and sapphire). SEM images: the surface of the films and cross section for thickness determination were recorded with a JEOL JSM 7001F electron microscope for all samples in GEMaC and IEMN. Example of SEM image of cross section for undoped and Zn:doped films grown on Si substrate shown in Fig. 4.

The crystallographic structure of the films was analyzed by X-ray diffraction (XRD) with a Siemens D-5000 diffractometer using Cu-K_α radiation ($\lambda = 1.54$ Å). Secondary-ion mass spectrometry (SIMS) were used for in-depth Ga, Zn, O profiles, using a Cameca IMS 4f equipment. TEM cross-sections were prepared by conventional mechanical polishing and ion milling. Electron energy loss spectroscopy (EELS) spectrum images and profiles were obtained in high angle annular dark-field (HAADF) STEM mode with an EDAX super ultra-thin window (SUTW) X-ray detector a Gatan Quantum SE 963 imaging filter respectively.

Ohmic contacts for undoped and doped samples grown of sapphire substrate were prepared by silver paint at the four corners of the sample. Sample were connected by gold wires in the measurement cell. I–V characterization to verify Ohmicity of the electrical contacts were carried out at different temperatures. Hall Effect measurements were performed in a Van der Pauw configuration in the temperature range of 80K–850K and for magnetic fields perpendicular to the film plane varying from −1.6 T to 1.6 T, using a high impedance measurement set-up which was custom designed for measurement of high resistance samples.

Ti (400)/Au (200) nm metal contacts of 170 μm × 300 μm size were evaporated on Ga_2O_3 and Zn:Ga_2O_3 films grown on Si (111) substrates. The contact is not Ohmic (at room temperature), though there is no influence of the contact nature on the vertical breakdown of the film as seen from other wide bandgap such as GaN or SiC.

A Keysight B1505A Power Device Analyzer has been used in order to carry out the vertical breakdown measurements. Bias voltages have been applied on an isolated Ohmic contact with the substrate grounded in order to access the breakdown voltage.

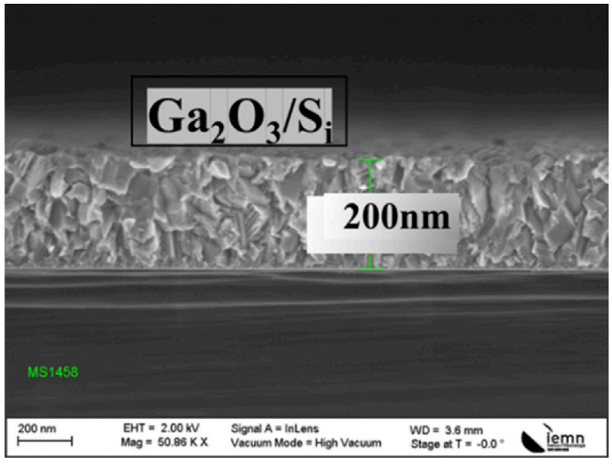

Fig. 4. SEM image of cross section for undoped Ga_2O_3 films grown on Si(111) substrate.

Author contribution

Dr.Ekaterine Chikoidze: Conceptualization; Supervision, Electrical Measurements; Validation; Writing – original draft.

Dr.Tamar Tchelidze: Thermodynemic calculations; Investigation; Electrical field calculations.

Dr. Corinne Sartel: MOCVD growth; SEM images.

Zeyu Chi (mater student): Hall Effect measurements and data curation; State of the art writing.

Dr.Riad Kabouche: Electrical contact deposition; Break down electrical measurements; data curation.

Ismail Madaci (PhD **student)**:Hall Effect measurements; Data curation.

Dr.Carles Rubio:TEM analyses.

Hagar Mohamed(PhD student): XRD measurements; structural analysis.

Dr.Vincent Sallet: MOCVD growth; validation of the samples.

Dr. Farid Medjdoub: Break down electrical measurements ;validation.

Dr.Amador Perez-Tomas: Conceptualization; Investigation;-Writing – review & editing.

Dr.Yves Dumont: Investigation; Writing – review & editing.

Declaration of competing interest

The authors declare that they have no known competing financial interests or personal relationships that could have appeared to influence the work reported in this paper.

Acknowledgments

We acknowledge Dr. F. Jomard (GEMaC) for SIMS measurements. Hagar Mohammed would like to acknowledge Cultural Affairs and Massion Sector, Egyptian Ministry for Higher Education for her fellowship giving possibility work in France. APT acknowledges Agencia Estatal de Investigación (AEI) and Fondo Europeo de Desarrollo Regional (FEDER) under contract ENE2015-74275-JIN. The ICN2 is funded by the CERCA programme/Generalitat de Catalunya and by the Severo Ochoa programme of the Spanish Ministry of Economy, Industry and Competitiveness (MINECO, grant no. SEV-2017-0706).

References

[1] J. Millán, P. Godignon, X. Perpiñà, A. Pérez-Tomás, J. Rebollo, A Survey of Wide

Bandgap Power Semiconductor Devices, 2014, pp. 2155–2163, https://doi.org/10.1109/TPEL.2013.2268900.
[2] B.J. Baliga, Fundamentals of Power Semiconductor Devices, Springer, New York, NY, 2008.
[3] A. Perez-Tomas, E. Chikoidze, Michael R. Jennings, Stephen A.O. Russell, Ferechteh H. Teherani, Philippe Bove, Eric V. Sandana, David J. Rogers, Wide and ultra-wide bandgap oxides:where paradigm-shift photovoltaicsmeets transparent power electronics, IX, 105331Q, Proc. SPIE 10533 (2018), https://doi.org/10.1117/12.2302576.
[4] S.M. Sze, G. Gibbons, Avalanche breakdown voltages of abrupt and linearly graded p-n junctions in Ge, Si, GaAs, and Gap, Appl. Phys. Lett. 8 (1966) 111–113, https://doi.org/10.1063/1.1754511.
[5] M. Higashiwaki, K. Sasaki, A. Kuramata, T. Masui, S. Yamakoshi, Gallium oxide (Ga 2O 3) metal-semiconductor field-effect transistors on single-crystal β-Ga 2O 3 (010) substrates, Appl. Phys. Lett. 100 (2012) 1–4, https://doi.org/10.1063/1.3674287.
[6] K. Ghosh, U. Singisetti, Impact ionization in β-Ga2O3, J. Appl. Phys. 124 (2018), https://doi.org/10.1063/1.5034120.
[7] G. Irudayadass, J. Shi, The estimation of impact ionization coefficients for β-$-Ga$_{2}O_{3}$ 1 (2018) 1–7.
[8] X. Li, H.L. Lu, H.P. Ma, J.G. Yang, J.X. Chen, W. Huang, Q. Guo, J.J. Feng, D.W. Zhang, Chemical, optical, and electrical characterization of Ga2O3 thin films grown by plasma-enhanced atomic layer deposition, Curr. Appl. Phys. 19 (2019) 72–81, https://doi.org/10.1016/j.cap.2018.11.013.
[9] D.J. Robbins, Aspects of the theory of impact ionization in semiconductors (III), Phys. Status Solidi 98 (1980) 11–36, https://doi.org/10.1002/pssb.2220980102.
[10] A.G. Chynoweth, Uniform silicon p-n junctions. II. Ionization rates for electrons, J. Appl. Phys. 31 (1960) 1161–1165, https://doi.org/10.1063/1.1735795.
[11] W. Fulop, Calculation of avalanche breakdown voltages of silicon p-n junctions, Solid State Electron. 10 (1967) 39–43, https://doi.org/10.1016/0038-1101(67)90111-6.
[12] L. V Keldysh, Kinetic theory of impact ionization in semiconductors, J. Exp. Theor. Phys. 37 (1960) 713–727.
[13] L. Keldysh, Concerning the theory of impact ionization in semiconductors, Soviet Journal of Experimental and Theoretical Physics 21 (1965) 1135.
[14] L. Bourgoin, M. Lannoo, Point Defects in Semiconductors II Experimental Aspects, Springer Series in Solid-State Sciences, 1983, https://doi.org/10.1017/CBO9781107415324.004.
[15] B. Jayant Baliga, Wide Bandgap Semiconductor Power Devices, Elsevier, 2018, https://doi.org/10.1016/B978-0-08-102306-8.00001-0.
[16] C. Li, J.L. Yan, L.Y. Zhang, G. Zhao, Electronic structures and optical properties of Zn-doped β-Ga 2O3 with different doping sites, Chin. Phys. B 21 (2012) 1–6, https://doi.org/10.1088/1674-1056/21/12/127104.
[17] C. Zhang, F. Liao, X. Liang, H. Gong, Q. Liu, L. Li, X. Qin, X. Huang, C. Huang, Electronic transport properties in metal doped beta-Ga2O3: a first principles study, Phys. B Condens. Matter 562 (2019) 124–130, https://doi.org/10.1016/j.physb.2019.03.004.
[18] A. Kyrtsos, M. Matsubara, E. Bellotti, On the feasibility of p-type Ga2O3, Appl. Phys. Lett. 112 (2018), https://doi.org/10.1063/1.5009423.
[19] C. Tang, J. Sun, N. Lin, Z. Jia, W. Mu, X. Tao, X. Zhao, Electronic structure and optical property of metal-doped Ga2O3: a first principles study, RSC Adv. 6 (2016) 78322–78334, https://doi.org/10.1039/c6ra14010f.
[20] L. Zhang, J. Yan, Y. Zhang, T. Li, X. Ding, A comparison of electronic structure and optical properties between N-doped β-Ga 2O 3 and NZn co-doped β-Ga 2O 3, Phys. B Condens. Matter 407 (2012) 1227–1231, https://doi.org/10.1016/j.physb.2012.01.107.
[21] Y. Guo, H. Yan, Q. Song, Y. Chen, S. Guo, Electronic structure and magnetic interactions in Zn-doped β-Ga 2O3 from first-principles calculations, Comput. Mater. Sci. 87 (2014) 198–201, https://doi.org/10.1016/j.commatsci.2014.02.020.
[22] W. Yue, J. Yan, J. Wu, L. Zhang, Structural and optical properties of Zn-doped β-Ga 2O 3 films, J. Semiconduct. 33 (2012) 3–6, https://doi.org/10.1088/1674-4926/33/7/073003.
[23] D. Guo, X. Qin, M. Lv, H. Shi, Y. Su, G. Yao, S. Wang, C. Li, P. Li, W. Tang, Decrease of oxygen vacancy by Zn-doped for improving solar-blind photoelectric performance in β-Ga2O3 thin films, Elec Mat Lett 13 (2017) 483–488, https://doi.org/10.1007/s13391-017-7072-y.
[24] J. Tao, H.L. Lu, Y. Gu, H.P. Ma, X. Li, J.X. Chen, W.J. Liu, H. Zhang, J.J. Feng, Investigation of growth characteristics, compositions, and properties of atomic layer deposited amorphous Zn-doped Ga 2 O 3 films, Appl. Surf. Sci. 476 (2019) 733–740, https://doi.org/10.1016/j.apsusc.2019.01.177.
[25] X.H. Wang, F.B. Zhang, K. Saito, T. Tanaka, M. Nishio, Q.X. Guo, Electrical properties and emission mechanisms of Zn-doped β-Ga 2O3 films, J. Phys. Chem. Solid. 75 (2014) 1201–1204, https://doi.org/10.1016/j.jpcs.2014.06.005.
[26] Y. Li, A. Trinchi, W. Wlodarski, K. Galatsis, K. Kalantar-Zadeh, Investigation of the oxygen gas sensing performance of Ga2O3 thin films with different dopants, Sensor. Actuator. B Chem. 93 (2003) 431–434, https://doi.org/10.1016/S0925-4005(03)00171-0.
[27] E. Chikoidze, A. Fellous, A. Perez-Tomas, G. Sauthier, T. Tchelidze, C. Ton-That, T.T. Huynh, M. Phillips, S. Russell, M. Jennings, B. Berini, F. Jomard, Y. Dumont, P-type β-gallium oxide: a new perspective for power and optoelectronic devices, Mat Tod Physf 3 (2017) 118–126, https://doi.org/10.1016/j.mtphys.2017.10.002.
[28] E. Chikoidze, C. Sartel, H. Mohamed, I. Madaci, T. Tchelidze, M. Modreanu, P. Vales-Castro, C. Rubio, C. Arnold, V. Sallet, Y. Dumont, A. Perez-Tomas, Enhancing the intrinsic p-type conductivity of the ultra-wide bandgap Ga2O3 semiconductor, J. Mater. Chem. C. 7 (2019) 10231, https://doi.org/10.1039/C9TC02910A.
[29] E. Chikoidze, C. Sartel, I. Madaci, H. Mohamed, C. Vilar, B. Ballesteros, F. Belarre, E. del Corro, P. Vales-Castro, G. Sauthier, L. Li, M. Jennings, V. Sallet, Y. Dumont, A. Perez-Tomas, P-type ultra-wide bandgap spinel ZnGa2O4: new perspectives for energy electronics, Cryst. Growth Des. (2020), https://doi.org/10.1021/acs.cgd.9b01669 acs.cgd.9b01669.
[30] F. Alema, B. Hertog, O. Ledyaev, D. Volovik, G. Thoma, R. Miller, A. Osinsky, P. Mukhopadhyay, S. Bakhshi, H. Ali, W.V. Schoenfeld, Solar blind photodetector based on epitaxial zinc doped Ga2O3 thin film, Physica Status Solidi (A) Applications and Materials Science (2017) 214, https://doi.org/10.1002/pssa.201600688.
[31] N.K. Shrestha, K. Lee, R. Kirchgeorg, R. Hahn, P. Schmuki, Self-organization and zinc doping of Ga2O3 nanoporous architecture: a potential nano-photogenerator for hydrogen, Electrochem. Commun. 35 (2013) 112–115, https://doi.org/10.1016/j.elecom.2013.08.011.
[32] Y. Sakata, Y. Matsuda, T. Yanagida, K. Hirata, H. Imamura, K. Teramura, Effect of metal ion addition in a Ni supported Ga2O3 photocatalyst on the photocatalytic overall splitting of H2O, Catal. Lett. 125 (2008) 22–26, https://doi.org/10.1007/s10562-008-9557-7.
[33] Q. Feng, J. Liu, Y. Yang, D. Pan, Y. Xing, X. Shi, X. Xia, H. Liang, Catalytic growth and characterization of single crystalline Zn doped p-type β-Ga2O3nanowires, J. Alloys Compd. 687 (2016) 964–968, https://doi.org/10.1016/j.jallcom.2016.06.274.
[34] F.A. Kroger, The Chemistry of Imperfect Crystals, North-Holland, Amsterdam, Interscience (Wiley), New York, 1964, https://doi.org/10.1002/bbpc.19640680615.
[35] R.L. Longini, Rapid zinc diffusion in gallium arsenide, Solid State Electron. 5 (1962) 127–130, https://doi.org/10.1016/0038-1101(62)90002-3.
[36] G.F. Neumark, Are impurities the cause of "self"-compensation in large-band-gap semiconductors? J. Appl. Phys. 51 (1980) 3383–3387, https://doi.org/10.1063/1.328051.
[37] H.W. Kim, N.H. Kim, C. Lee, Growth of Ga2O3 thin films on Si(100) substrates using a trimethylgallium and oxygen mixture, J. Mater. Sci. 39 (2004) 3461–3463, https://doi.org/10.1023/B:JMSC.0000026951.53297.e8.
[38] Y. Chen, H. Liang, X. Xia, R. Shen, Y. Liu, Y. Luo, G. Du, Effect of growth pressure on the characteristics of β-Ga 2 O 3 films grown on GaAs (100) substrates by MOCVD method, Appl. Surf. Sci. 325 (2015) 258–261, https://doi.org/10.1016/j.apsusc.2014.11.074.
[39] Y. Takiguchi, S. Miyajima, Effect of post-deposition annealing on low temperature metalorganic chemical vapor deposited gallium oxide related materials, J. Cryst. Growth 468 (2017) 129–134, https://doi.org/10.1016/j.jcrysgro.2016.11.005.
[40] H.W. Kim, N.H. Kim, C. Lee, Structural and optical properties of annealed Ga2O3 films on Si(111) substrates, Br. Ceram. Trans. 103 (2004) 187–189, https://doi.org/10.1179/096797804225018741.
[41] H.W. Kim, N.H. Kim, Growth of gallium oxide thin films on silicon by the metal organic chemical vapor deposition method, Mater. Sci. Eng. B: Solid-State Materials for Advanced Technology 110 (2004) 34–37, https://doi.org/10.1016/j.mseb.2004.01.012.
[42] H.W. Kim, N.H. Kim, Formation of amorphous and crystalline gallium oxide nanowires by metalorganic chemical vapor deposition, Appl. Surf. Sci. 233 (2004) 294–298, https://doi.org/10.1016/j.apsusc.2004.03.262.
[43] D.H. Kim, S.H. Yoo, T.M. Chung, K.S. An, H.S. Yoo, Y. Kim, Chemical vapor deposition of Ga2O3 thin films on Si substrates, Bull. Kor. Chem. Soc. 23 (2002) 225–228, https://doi.org/10.5012/bkcs.2002.23.2.225.
[44] C.V. Ramana, E.J. Rubio, C.D. Barraza, A. Miranda Gallardo, S. McPeak, S. Kotru, J.T. Grant, Chemical bonding, optical constants, and electrical resistivity of sputter-deposited gallium oxide thin films, J. Appl. Phys. 115 (2014), https://doi.org/10.1063/1.4862186.
[45] H. Altuntas, I. Donmez, C. Ozgit-Akgun, N. Biyikli, Electrical characteristics of β-Ga2O3 thin films grown by PEALD, J. Alloys Compd. 593 (2014) 190–195, https://doi.org/10.1016/j.jallcom.2014.01.029.
[46] A. Mock, J. VanDerslice, R. Korlacki, J.A. Woollam, M. Schubert, Elevated temperature dependence of the anisotropic visible-to-ultraviolet dielectric function of monoclinic β -Ga $_2$ O $_3$, Appl. Phys. Lett. 112 (2018): 041905, https://doi.org/10.1063/1.5010936.
[47] S.J. Pearton, J. Yang, F. Ren, J. Kim, Progress in Semiconductor β-Ga2O3, 2019, https://doi.org/10.1016/b978-0-12-815468-7.00003-2.